Understanding of European Cold Extremes, Sudden Stratospheric Warming, and Siberian Snow Accumulation in the Winter of 2017/18

ZHUOZHUO LÜ

Nansen-Zhu International Research Centre, Institute of Atmospheric Physics, Chinese Academy of Sciences, and University of Chinese Academy of Sciences, Beijing, China

FEI LI

Geophysical Institute, University of Bergen and Bjerknes Centre for Climate Research, Bergen, Norway

YVAN J. ORSOLINI

Norwegian Institute for Air Research (NILU), Kjeller, Norway

YONGQI GAO

Nansen Environmental and Remote Sensing Center and Bjerknes Centre for Climate Research, Bergen, Norway, and Nansen-Zhu International Research Centre, Institute of Atmospheric Physics, Chinese Academy of Sciences, Beijing, China

SHENGPING HE

Geophysical Institute, University of Bergen, and Bjerknes Centre for Climate Research, Bergen, Norway

(Manuscript received 14 December 2018, in final form 30 September 2019)

ABSTRACT

It is unclear whether the Eurasian snow plays a role in the tropospheric driving of sudden stratospheric warming (SSW). The major SSW event of February 2018 is analyzed using reanalysis datasets. Characterized by predominant planetary waves of zonal wave 2, the SSW developed into a vortex split via wave–mean flow interaction. In the following two weeks, the downward migration of zonal-mean zonal wind anomalies was accompanied by a significant transition to the negative phase of the North Atlantic Oscillation, leading to extensive cold extremes across Europe. Here, we demonstrate that anomalous Siberian snow accumulation could have played an important role in the 2018 SSW occurrence. In the 2017/18 winter, snow depths over Siberia were much higher than normal. A lead–lag correlation analysis shows that the positive fluctuating snow depth anomalies, leading to intensified ''cold domes'' over eastern Siberia (i.e., in a region where the climatological upward planetary waves maximize), precede enhanced wave-2 pulses of meridional heat fluxes (100 hPa) by 7–8 days. The snow–SSW linkage over 2003–19 is further investigated, and some common traits among three split events are found. These include a time lag of about one week between the maximum anomalies of snow depth and wave-2 pulses (100 hPa), high sea level pressure favored by anomalous snowpack, and a ridge anchoring over Siberia as precursor of the splits. The role of tropospheric ridges over Alaska and the Urals in the wave-2 enhancement and the role of Arctic sea ice loss in Siberian snow accumulation are also discussed.

1. Introduction

In late February of 2018, unusually cold snowy weather events occurred across Europe. Quite a few countries suffered from their worst winter ever: Belgium experienced its coldest day since 1901, and minimum temperatures of below −40°C were observed in many

Supplemental information related to this paper is available at the Journals Online website: https://doi.org/10.1175/JCLI-D-18-0861.s1.

Corresponding author: Zhuozhuo Lü, lvzhuozhuo16@mails.ucas.ac.cn

DOI: 10.1175/JCLI-D-18-0861.1

places in Sweden (Anadolu Agency 2018). Large-scale snowfall happened over southern Europe and even over the Mediterranean (Lapin 2018). The extensive cold spell caused severe destruction of life and property, resulting in more than 90 casualties (Ano plc 2018). Furthermore, energy supply, transportation, and emergency-response systems were seriously affected due to frigid temperatures and heavy snow.

Cold extremes in Europe are closely related to winter atmospheric circulation anomalies, including the North Atlantic Oscillation (NAO) and atmospheric blocking activities in the Atlantic–European region (e.g., Hurrell 1995; Thompson and Wallace 1998; Cattiaux et al. 2010; Sillmann et al. 2011; Pfahl 2014). A negative phase of the NAO (NAO−) is associated with an enhanced northerly or easterly wind, higher atmospheric blocking occurrences, and unusual low temperatures over much of Europe (Lamb and Peppler 1987; Moses et al. 1987; Cheung et al. 2016). Such blockings can induce strong cold advection associated with anomalous surface easterlies (Takaya and Nakamura 2005), and the numbers of cold spell days are closely linked with the duration and frequency of blocking events over Europe (Buehler et al. 2011).

In mid-February 2018 a major sudden stratospheric warming (SSW) event occurred (see Fig. 3 and section 3a for details). Major SSW events (SSWs) are characterized by a rapid reversal of the circumpolar stratospheric westerlies and a dramatic warming of polar stratospheric temperature over a short time period (Butler et al. 2015). As the clearest and strongest manifestation of coupling in the stratosphere–troposphere system, SSWs can drive changes in surface climate on time scales of days to weeks (Charlton and Polvani 2007; Mitchell et al. 2013; Kidston et al. 2015). Following an SSW event, the weakened stratospheric polar vortex can contribute to an NAO− pattern and increase the frequency of cold air outbreaks over Eurasia and North America (Kidston et al. 2015; Butler et al. 2017).

The causes of interannual variability in SSWs are still under debate. It has long been understood that strong upward-propagating planetary waves (PWs) from the troposphere into the stratosphere perturb the circumpolar westerlies and induce the occurrence of SSWs (Matsuno 1971; Andrews et al. 1987; Polvani and Waugh 2004). Early studies have indicated that both the tropical ocean/El Niño–Southern Oscillation (ENSO) and extratropical ocean are strong stationary planetary wave sources (Chen et al. 2003; Manzini et al. 2006; Li et al. 2015). In addition, the land component of the climate system also plays a significant role in forcing the wintertime atmospheric circulation, such as Eurasian snow cover (Cohen and Entekhabi 1999). Recently, a growing body of studies has reinvestigated the linkages between high-latitude snow cover and the stratospheric variability in order to improve atmospheric forecast skill on subseasonal time scales (e.g., Furtado et al. 2016; Orsolini et al. 2016; Li et al. 2018, 2019). As one of the most variable land surface conditions in time and space in the Northern Hemisphere (NH), the prediction potential of snow cover deserves further investigation. Using lead–lag correlation methods applied to reanalyses and model studies, Cohen and collaborators (e.g., Cohen et al. 2007, 2010, 2014a,b), Saito et al. (2001), Saito and Cohen (2003), and Gong et al. (2003) have highlighted a dynamical pathway by which the upward PWs, which emanate from the extensive Eurasian snow cover, lead to a weakened polar vortex and subsequent negative NAO/Arctic Oscillation (AO). By performing retrospective forecasts in early winter of 2009/10 with coupled ocean–atmosphere seasonal forecast model, Orsolini et al. (2016) investigated the linkage between snow initial conditions and the maintenance of NAO− via a troposphere–stratosphere coupling operating on a time scale of two weeks. Zhang et al. (2016) also proposed that a recent shifting of Arctic polar vortex toward the Eurasian continent is likely linked to the increased Eurasian snow cover.

In spite of numerous efforts to explore the prime tropospheric factors that drive SSWs, there has been a debate on the role of Eurasian snow (e.g., Cohen et al. 2005; Limpasuvan et al. 2005). There also remains a debate on whether the autumn snow cover impacts the winter-mean NAO/AO (e.g., Henderson et al. 2018). Douville et al. (2017) revisited the relationship between October snow and winter-mean NAO/AO based on two twentieth-century reanalysis datasets. They pointed that this linkage was not robust across the twentieth century. Hence, while atmospheric models readily respond to a large prescribed or initial Eurasian snow autumn anomalies (Fletcher et al. 2009; Peings et al. 2012; Orsolini et al. 2016), the impact of snow cover on actual SSWs or on the winter-mean NAO/AO remains unclear.

In this study, we investigated the evolution and causes of the SSW event in February 2018 and its linkage with cold extremes across Europe. We suggest that rapid anomalous snow accumulation over Siberia played a key role in the occurrence of this major stratospheric warming. Differing from the extensive studies that demonstrated the impact of snow on the winter stratosphere on seasonal time scales, our research provides insight on synoptic and subseasonal time scales. The linkage between snow depth anomalies and the SSW event is analyzed on daily time scales using reanalysis data.

2. Reanalyses and methods

The atmospheric data are obtained from the National Centers for Environmental Prediction (NCEP)–U.S.

Department of Energy (DOE) Atmospheric Model Intercomparison Project phase II (AMIP-II) reanalysis dataset (NCEP R2; Kanamitsu et al. 2002), including daily mean air temperature at 2 m (T2m), mean sea level pressure (SLP), surface pressure, zonal and meridional winds at 10 m, and temperature, geopotential height, zonal and meridional winds, and relative humidity from 1000 to 10 hPa. The daily snow depths used in this study are derived from the snow water equivalent data from the European Centre for Medium-Range Weather Forecasts (ECMWF) interim reanalysis dataset (ERA-Interim; Dee et al. 2011). Daily NAO index is taken from http://www.cpc.ncep.noaa.gov/products/precip/CWlink/pna/nao.shtml.

Daily anomalies are calculated by removing the daily climatological mean (mean of 1979–2017) from the original data. Here the climatological mean is previously smoothed by retaining the first four temporal Fourier coefficients of the raw daily mean climatology, with low-frequency variability preserved (e.g., Wilks 2006). Prior to 2003, snow analyses in ERA-Interim are based on in situ observations of snow depth, without assimilation of satellite data. After 2003, with the assimilation of the satellite-based NOAA/NESDIS daily snow cover data, the ERA-Interim snow analyses have considerably improved in terms of interannual variability (Dee et al. 2011; Orsolini et al. 2013). Because of the limitations of the dataset quality, the climatology of the snow depth is calculated for the period of 2003–17.

Here we define a cold extreme when the daily T2m anomaly is below the calendar day 10th percentile, which is calculated using the anomalies from five consecutive days centered on the day of interest over the 39 years (1979–2017), following a method described in Zhang et al. (2005) [see their Eq. (1)]. Similarly, the calculation of extreme trough (ridge) pattern is based on the 10th (90th) percentiles for 500-hPa geopotential height (Z500). According to the World Meteorological Organization (WMO) definition, an SSW is called minor if polar temperature increases by least 25° in a period of a week or less at any stratospheric level. Further, an SSW is major if the latitudinal mean temperature increases poleward from 60° latitude and an associated circulation reversal is observed at 10 hPa or below (McInturff 1978, p. 19). The first day on which the zonal-mean zonal wind at 60°N and 10 hPa becomes easterly is defined as the central date of the SSW. In addition, only major SSW events occurring from 1 December until 15 March are considered, because our analyses focus on wintertime and stratospheric final warmings are discarded.

The wave activity flux (WAF; Plumb 1985) is used to provide the propagation features of quasi-stationary Rossby waves. Moreover, the Eliassen–Palm (EP) flux (Andrews et al. 1987) is adopted as a diagnostic tool to measure the wave heat and momentum propagation in the meridional plane. An equatorward (upward) EP flux is proportional to poleward meridional eddy momentum (heat) flux. The statistical significances are assessed using a Monte Carlo approach based on 10 000 random reshufflings of the observational anomalies.

3. Analysis of 2017/18 winter

a. *The European cold extremes in late February 2018 and associated major sudden stratospheric warming event*

Figures 1 and 2 show the spatial development of extreme low T2m and high/low Z500 from 23 to 28 February, respectively. Pronounced cold extremes began to appear over western Russia on 23 February, extending westward in the following 6 days and peaking on 26–27 February over most of Europe, western Russia, and parts of central Russia (Fig. 1). Concurrently, we note that the pronounced ridge located on 23 February over the Barents–Kara Sea and the Nordic seas extended westward later (Fig. 2), which might favor a weakened westerly regime and prolonged the duration of wintry conditions in Europe. Besides, the near-surface anticyclonic circulations over the European Arctic advected cold air from the Arctic Ocean and Siberia to Europe, leading to widespread cold air outbreaks (see Fig. S1 in the online supplemental material). Figure 2 also reveals a pronounced anticyclonic anomaly over the North Pacific, south of Alaska, which will be discussed later.

Figure 3 shows the daily evolution of zonal-mean temperature and zonal wind at 10 hPa from 1 January to 15 March 2018. Before 10 February, the 10-hPa zonal-mean temperatures were found below 220 K poleward of 70°N (Fig. 3a), accompanied by the maximum 10-hPa westerlies in excess of 40 m s^{-1} around 65°N (Fig. 3b). From 11 February, there was a warming event, in which the temperatures quickly increased above 240 K over the polar region north of 65°N. Meanwhile, the zonal wind reversed rapidly (i.e., decelerated) and attained a magnitude of -30 m s^{-1}. This warming pulse lasted for approximately 20 days and can be identified as a major SSW event (SSW18 hereafter), with its central date on 11 February 2018.

The spatial structure of the polar vortex on 9, 11, 13, and 15 February 2018 is presented in Fig. 4 using geopotential height and potential vorticity at 10 hPa, both of which can be used to identify the types of SSW events (Seviour et al. 2013). Two days before the central date (Fig. 4a), the North Pole was characterized by a distorted polar vortex, with developed troughs over western Siberia and North America and two highs on its flanks. Subsequently, the polar vortex began to split into

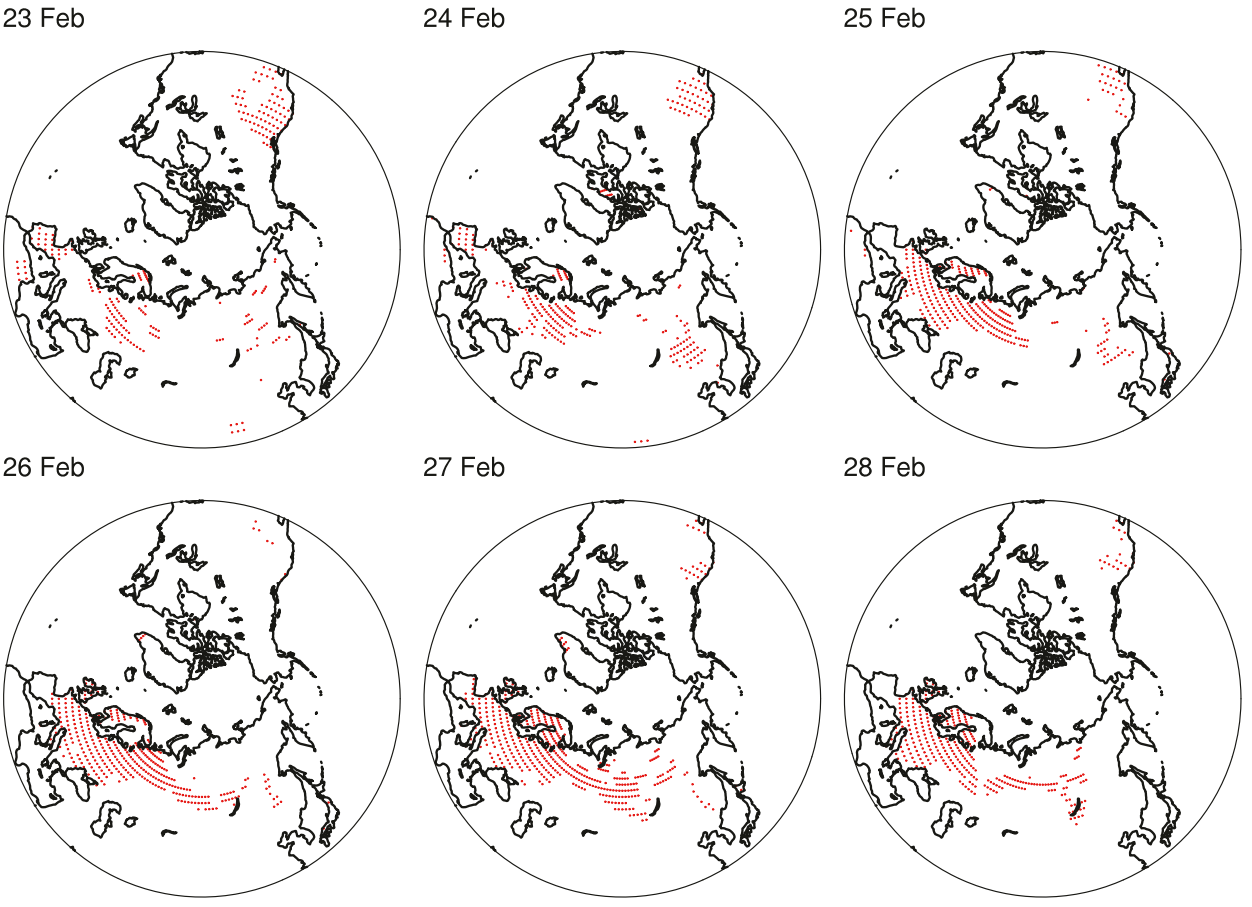

FIG. 1. The spatial maps of daily cold extreme occurrence during 23–28 Feb 2018. The red dots indicate the coldest regions with temperature anomalies lower than 10th percentile thresholds.

two pieces: one centered over Canada, and the other migrating westward from central Eurasia to western Europe between 11 and 15 February (Figs. 4b–d).

The massive anticyclone and split vortices induced the zonal-mean zonal wind reversal, followed by apparent downward propagation of zonal-mean circulation anomalies from the stratosphere to the troposphere. The time–pressure cross section of zonal-mean zonal wind (temperature) anomalies over polar region is further presented in Fig. 5a (Fig. S2). In early January westerly wind anomalies dominated throughout the stratosphere. Then the first planetary wave pulse peaking in mid-January (16 January) decelerated the polar vortex, leading to a minor warming. After a recovery of the westerlies, the large second pulse in early February followed, corresponding to strong poleward heat transport (see Fig. 5b), which led to a lasting reversal to easterlies and to the major warming. The reversal occurred nearly simultaneously throughout the stratosphere from 10 to 200 hPa. Then, in late February, the negative zonal wind anomalies developed throughout the troposphere, and anomalous zonal-mean easterlies were found from 10 hPa down to the lower troposphere, consistent with the composite zonal wind anomalies during previous SSWs with significant transition to NAO− reaching the surface 15–20 days after the central date (Fig. S3) (Limpasuvan et al. 2004; Taguchi 2014; Orsolini et al. 2018).

Figures 6a–d show the temporal and spatial evolution of weekly mean SLP anomalies around and following the central date, and Figs. 6e and 6f present the temporal evolutions of the NAO index and the T2m anomaly index averaged over Europe. After the central date, the change in the distribution of SLP triggered the intraseasonal transition of NAO to its negative phase. The sequential Mann–Kendall test is used to detect monotonic trends and abrupt changes in the time series. As shown in Fig. 6e, the phase of NAO displays a significantly abrupt shift from positive to negative on 22 February. Correspondingly, the temperatures over Europe jumped to a minimum near the same time as the NAO index reached its minimum (Fig. 6f). Both indices decreased drastically, reaching their respective negative peaks on around

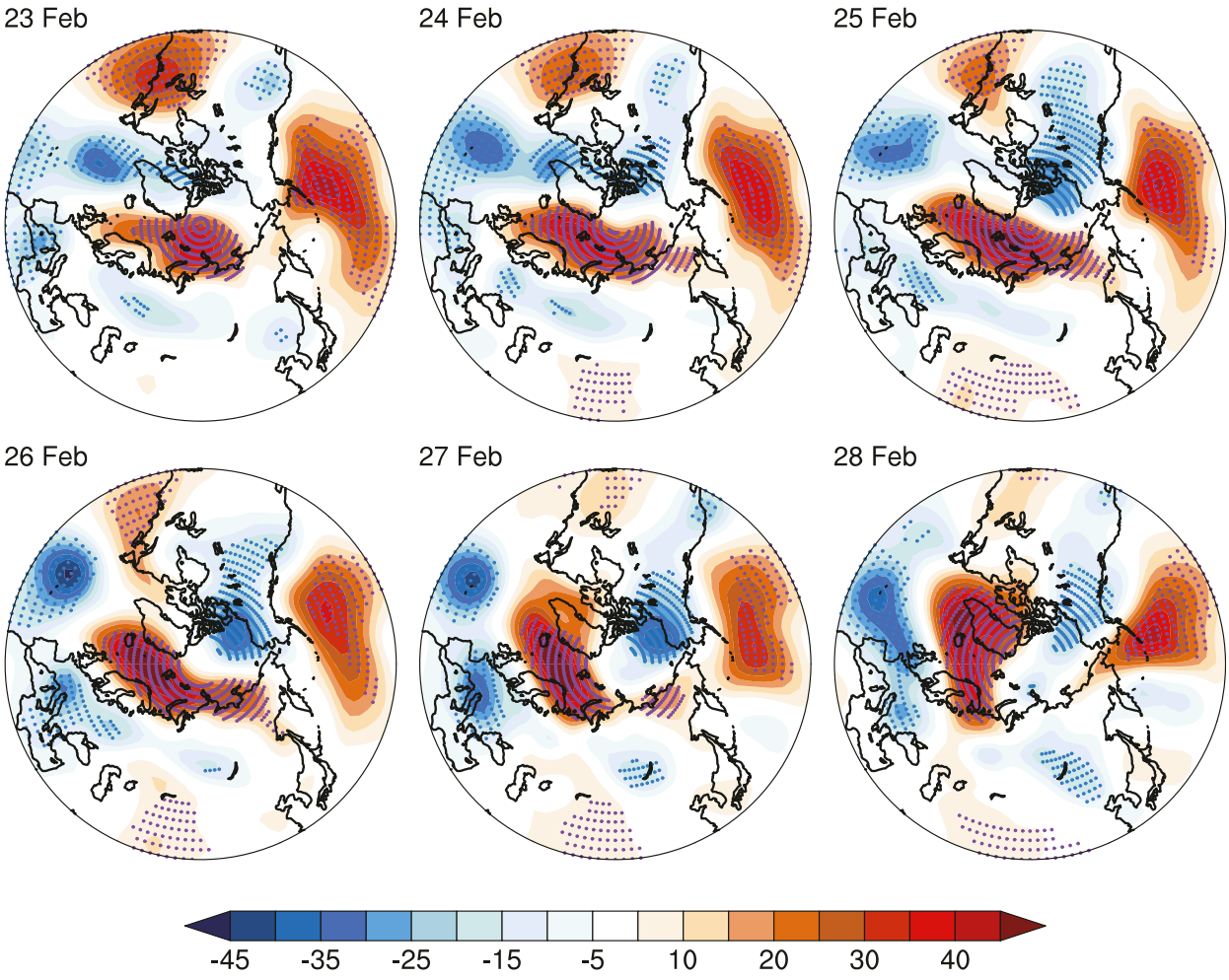

FIG. 2. The daily anomalies of geopotential height at 500 hPa (Z500; shading; gpm) during 23–28 Feb 2018. The purple (blue) dots denote the anomalies higher (lower) than 90th (10th) percentile thresholds.

26–28 February. The north–south dipole pattern of SLP anomalies took shape in late February across the Atlantic region and persisted into March (Figs. 6c,d), consistent with a downward influence from the stratosphere all the way to the surface (Fig. 5a). Ayarzagüena et al. (2018) showed that the transition to and persistence of the NAO− regime after SSW18 was unusual, characterized by an exceptional duration, significantly longer than climatology. Hence, SSW18 had remarkable tropospheric impacts, with the cold European conditions quickly built up within two weeks, and culminating with an unusual cold wave at the end of February.

b. Wave–mean flow interaction

A number of previous studies have linked weakened stratospheric polar vortex to upward-propagating PWs from the troposphere, especially zonal wave-1 and -2 components (e.g., Charlton and Polvani 2007; Nishii et al. 2011; Nath et al. 2016), whereas smaller-scale waves (i.e., wave 3 and larger numbers) are generally trapped near the tropopause (Charney and Drazin 1961; Andrews et al. 1987). Therefore, we first calculated the meridional eddy heat flux $v'T'$ and its wave-1 and wave-2 components at 100 hPa averaged over 30°–90°N (Fig. 5b). The term $v'T'$, where v and T are the meridional wind and temperature, respectively, and the prime denotes the deviation from the zonal mean, is proportional to the upward wave activity flux. Figure 5b is characterized by two dominant positive peaks (marked by the almond strips), with the primary one in early February and the secondary one in mid-January. The two peaks just correspond to the major warming and the preceding minor warming pulse shown in Fig. 5a. At its peak time, during the SSW18 event, the percentage of the wave-2 component to the total heat flux was found to be up to 62%, while the contribution of the wave-1 component was relatively weak.

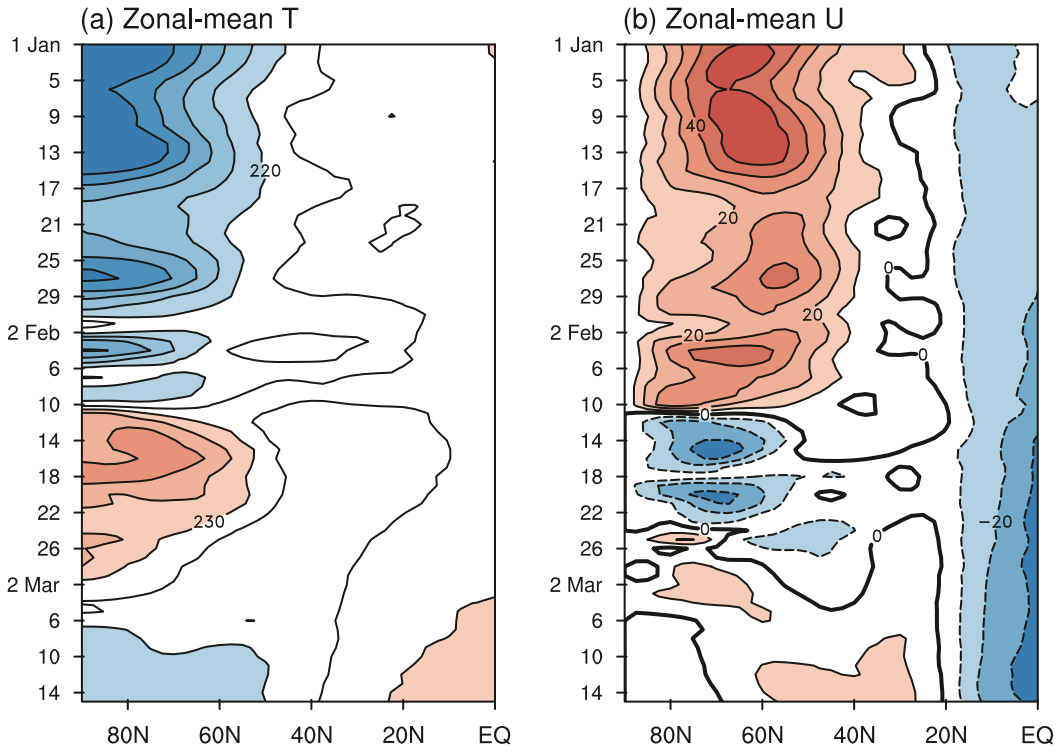

FIG. 3. Latitude–time cross sections of (a) zonal-mean temperature (contour interval: 5 K) and (b) zonal-mean zonal wind (contour interval: 10 m s^{-1}) at 10 hPa during 1 Jan–15 Mar 2018.

To identify the tropospheric wave source regions spatially and temporally in more detail, we divided the period of 20 January–14 February into seven tetrads. The left panels in Fig. 7 depict the longitude–pressure sections of 4-day mean WAF and geopotential height deviations from the zonal mean; in addition, horizontal distribution of the WAF and geopotential height anomalies are presented as maps in Fig. 8. The right panels in Fig. 7 show EP flux vectors overplotted on the accelerations of zonal-mean zonal winds. During 20–23 January (Figs. 7a and 8a), upward propagation of PWs can be mostly seen over the region of 60°–150°E and between 50° and 70°N (i.e., the location of Siberia). The pathway from the upper troposphere to the middle stratosphere appeared to have been preliminarily established; a pronounced stratosphere ridge was found over the region from 120°E to 120°W (Fig. 7a, left) and westerly deceleration was confined below the tropopause (Fig. 7a, right). During 24–27 and 28–31 January, enhanced waves emanating from Siberia maintained upward propagation into the stratosphere ridge; strengthened PWs propagated horizontally eastward toward the extratropical eastern Pacific (Figs. 7b,c, left; Figs. 8i,j). Subsequently, during 1–4 February (Fig. 7d), PWs continued propagating up into the stratosphere, although more weakly than in the previous tetrad. During 5–8 February (Fig. 7e), extensive upward PWs consistently dominated the stratosphere over the Eurasian longitudes. A wave-2 pattern appeared in the middle-upper troposphere, with a ridge at 60°–90°E developing rapidly, along with the pre-existing, eastward-migrating ridge near 150°W, forming a well-organized, westward-tilted wave-2 pattern that extended from the troposphere to the stratosphere (Figs. 7e and 8l). In their study of the vortex split event of 2009, Coy et al. (2011) also found that the amplifying wave 2 comprised a ridge near 60°–90°E, connected to the surface. During 9–14 February (Figs. 7f,g), strong upward PWs into the stratosphere led to a drastic weakening of the upper stratospheric westerlies, and finally the zonal winds reversed to easterly from the lower troposphere to the stratosphere poleward of 70°N (Fig. 7g, right). In addition, strong PW flux emanated from the developing tropospheric ridge near 150°W, propagating vertically and eastward toward the deepened trough near 80°W and the ridge downstream (Figs. 7f,g, left; Figs. 8m,n).

According to the analyses above, the evolution of SSW18 is characterized by the predominance of wave 2. Prior to the onset (from 15 to 0 days before the central date), the anomalous wave-2 pattern built from the troposphere to the stratosphere, nearly in phase with the climatological wave 2 (see Fig. S4a). Locking with the background climatological wave, the anomalous upward

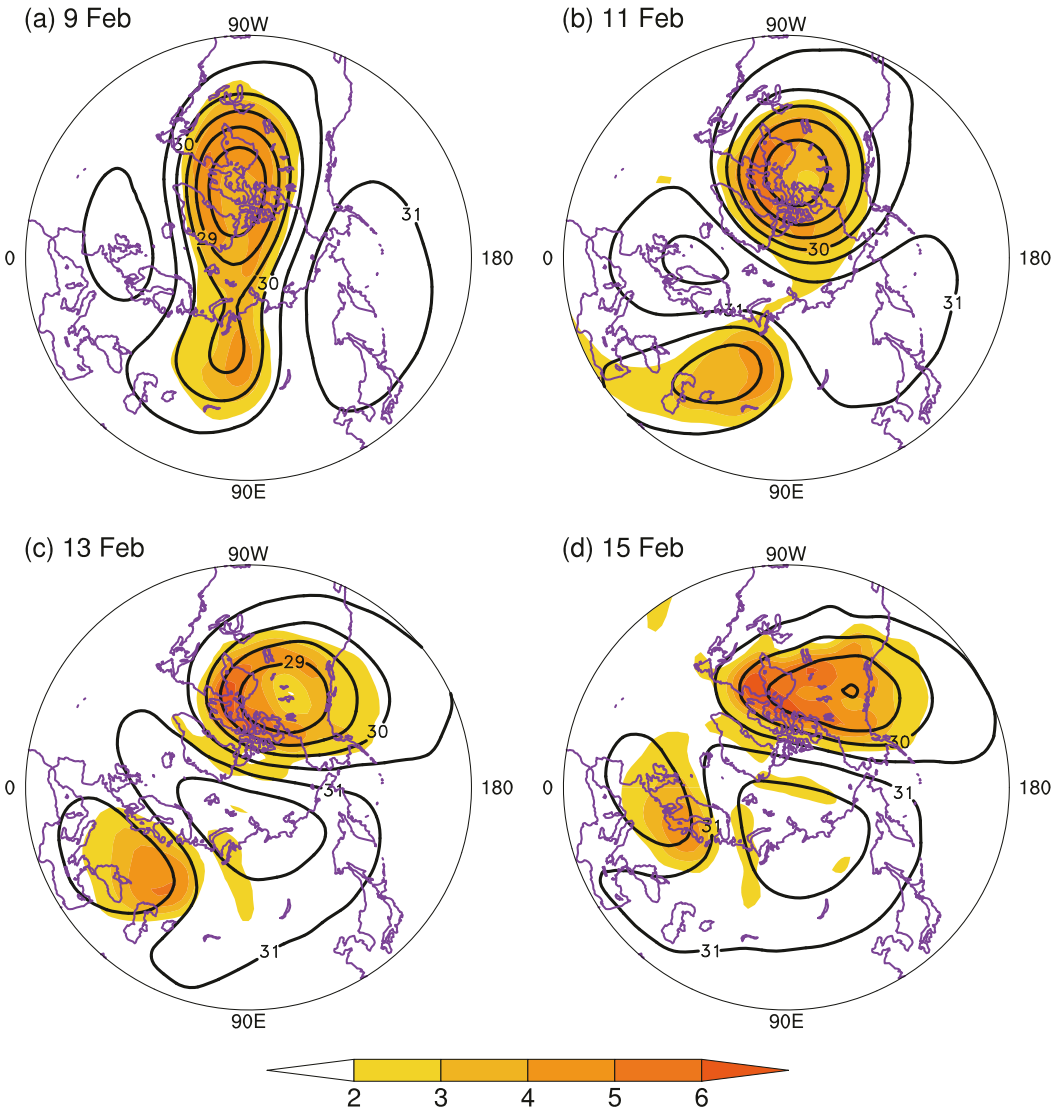

FIG. 4. Polar stereographic plot of geopotential height (contours; interval: 0.5 km) and potential vorticity (shading; 10^{-4} K kg^{-1} m^2 s^{-1}) on the 10-hPa pressure surface for (a) 9 Feb, (b) 11 Feb, (c) 13 Feb, and (d) 15 Feb 2018.

wave activity fluxes were amplified due to the constructive linear interference (Smith et al. 2011). The strong and persistent Rossby waves emanating from the Eurasian area (mainly over 30°–150°E) were the primary, consistent contributor for the upward tropospheric wave source. In particular, the increase of wave activity in the lower troposphere on 28–31 January triggered the enhanced upward PWs into the stratosphere.

c. *The role of Eurasian snow*

It is well known that the large variability of snow mass over Siberia exerts a strong influence on the surface energy budget and land–atmosphere coupling (Gong et al. 2004). Using hourly meteorological data, Betts et al. (2014) showed that temperature drops by 10 K over the Canadian Prairies following fresh snowfall during the winter transition. In the following, we primarily focus on whether the surface snow conditions contributed to the enhancement of upward-propagating PWs seen emanating from the boreal Eurasian continent prior to SSW18.

Figure 9 shows the monthly anomalies of snow depth and SLP over Eurasia from October 2017 to February 2018, along with anomalous integrated water vapor transport (WVT; integrated from the surface to 300 hPa). In late autumn (Figs. 9a,b), thicker snow depths were mainly located in the northeastern Eurasia, with enhanced moisture transport from the Barents–Kara Seas and the East Siberian–Chukchi Seas. During wintertime

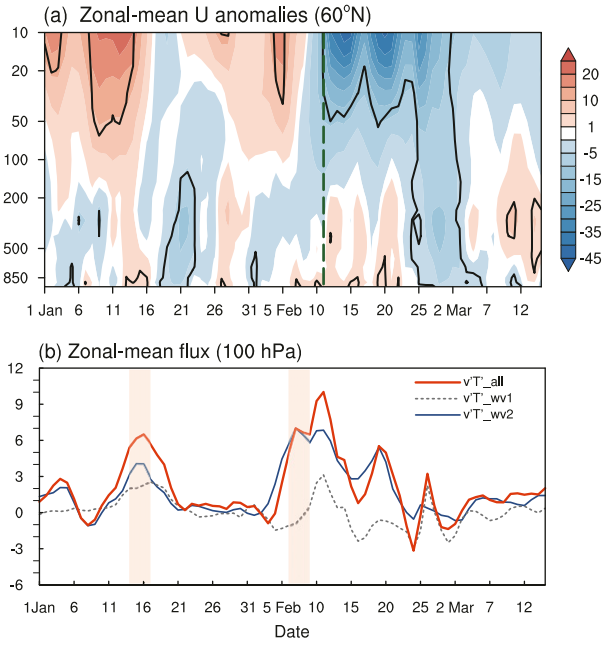

FIG. 5. (a) Time–pressure cross section of zonal-mean zonal wind anomalies (shading; m s^{-1}) at 60°N during 1 Jan–15 Mar 2018. The thick black contours indicate the 95% significance level, based on a Monte Carlo test. The dashed green line denotes the central date of SSW18. (b) Time series of zonal-mean eddy meridional heat flux (10 K m s^{-1}) for all wavenumbers ($v'T'$_all; red solid line), zonal wave 1 ($v'T'$_wv1; gray dashed line), and zonal wave 2 ($v'T'$_wv2; blue solid line) averaged over 30°–90°N at 100 hPa. The almond strips highlight the two major $v'T'$_wv2 maxima.

(Figs. 9c–e), coherent positive snow depth anomalies expanded over most territories of Siberia, with the maximum anomalies in western Siberia (to the east of the Urals). Actually, the early 2018 experienced near-record maximum snow accumulation over NH land areas, according to the 2018 snow assessment from the WMO's Global Cryosphere Watch (GCW) (https://globalcryospherewatch.org/assessments/snow/2018/). Associated with the extensive presence of Siberian snowpack, a positive SLP anomaly center dominated over central Eurasia, resembling the preferred precursor SLP pattern to enhanced vertical wave propagation as suggested by Cohen et al. (2014a). The transported moisture from the Arctic Ocean toward the adjacent northern lands increased in response to the widespread high pressure anomalies and this stronger northerly moisture flow might, in turn, favor thicker snow accumulation. In addition, as shown in all the seven tetrads in Figs. 8a–g, upward WAFz anomalies resided over the western–central Siberian region (where an upward climatological stationary wave center settles), coinciding with the significantly positive snow depth anomalies in January–February (Figs. 9d,e).

We further examine the lead–lag relationships between snow depths and vertical wave activity flux on daily time scales. Here the snow depth (SD) index is defined as the normalized sum of snow depth anomalies over the Siberian region (50°–72°N, 70°–170°E; the black frame in Fig. 9e). The daily varying SD index is presented in Fig. 10a, with the components with periods longer than 30 days removed. We focus on the period of 1 January–10 February, during which wave 2 turned out to be dominant and the two major positive wave pulses occurred (Fig. 5b). Figure 10b shows the lead–lag correlations between the daily SD index and the magnitude of the vertical EP flux (EPz) and its wave-2 component (EPz_wv2) at 100 hPa. Here the calculation of EPz and EPz_wv2 is exactly similar to that of $v'T'$ in section 3b except for normalization (see $v'T'$_all and $v'T'$_wv2 in Fig. 5b). The lead–lag relationship is not very sensitive to the exact definition of the enclosed areas for the SD index, several of which were tested and all of which produced qualitatively similar results. It can be seen that the SD leads the EPz and EPz_wv2, with upward wave activity peaking 7–8 days after a highest snow depth anomaly (see the two pairs of colored strips in Fig. 10a). The high lagged correlation coefficient between EPz and SD (approximately 0.9, even higher between EPz_wv2 and SD) suggests, along with previous analyses, that fluctuations in the anomalously thick Siberian snow may be efficient in forcing pulses of upward-propagating PWs. This correlation cannot truly assert causality, and it may be that the coincidental development of the two tropospheric ridges is the cause for both the anomalous snow over Siberia and the lagged SSW onset. Some mechanistic interpretation suggestive of a distinct role for the snow forcing, based on earlier work by Fletcher et al. (2009), is now discussed in detail.

In a general circulation model study with imposed snow perturbations, Fletcher et al. (2009) showed that the local diabatic cooling induced by the presence of snow over Siberia induces a cold dome and a raising of isentropes. This effect can be seen in Fig. 11: throughout the troposphere, an intensified cold dome can be seen over the Siberian region when contrasting the 4-day mean potential temperature during the period of high peak of SD (30 January–2 February) and the period before and after the peak (25–28 January and 7–10 February) (Figs. 11a,b). The doming increases with height, leading to relatively thick (less stable) isentropic layers locally (primarily between 70° and 150°E). Figure 11c presents the temporal evolution of the potential temperature averaged over 50°–72°N, 70°–150°E at 500 hPa, along with the SD index during 1 January–10 February 2018. The significant negative correlation ($r = -0.653$ for the corresponding 41-day series; above the 99% confidence level) supports that the snow-forced cooling raises isentropic surfaces rapidly (within 1–2 days; see the red and blue circle markers in Fig. 11c), strengthening the cold

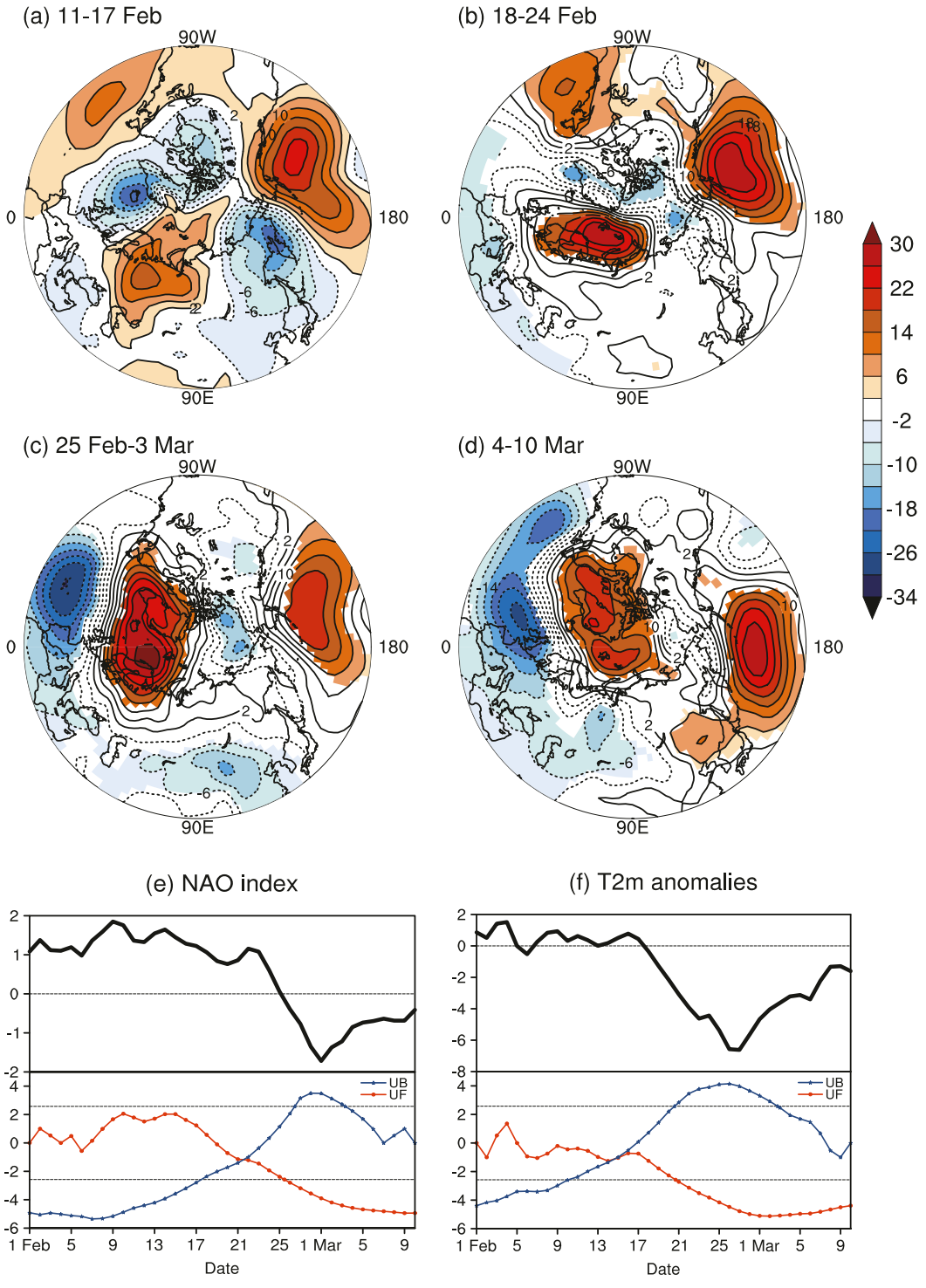

FIG. 6. SLP anomalies (hPa) for four successive 7-day means after the central date of SSW18. Dates are (a) 11–17 Feb, (b) 18–24 Feb, (c) 25 Feb–3 Mar, and (d) 4–10 Mar 2018. The SLP contours are shaded only where the statistical significance exceeds the 95% confidence level, based on a Monte Carlo test. (e) Time series of daily NAO index during 1 Feb–10 Mar 2018 (shown at top) and abrupt change in the NAO index as derived from the sequential Mann–Kendall test statistic (shown at bottom); UF is forward sequential statistic, UB is backward sequential statistic. The upper and lower dashed lines represent the confidence limits (at the 99% confidence level). (f) As in (e), but for the time series of the daily 2-m temperature anomalies (°C) averaged over the European region (40°–70°N, 0°–60°E).

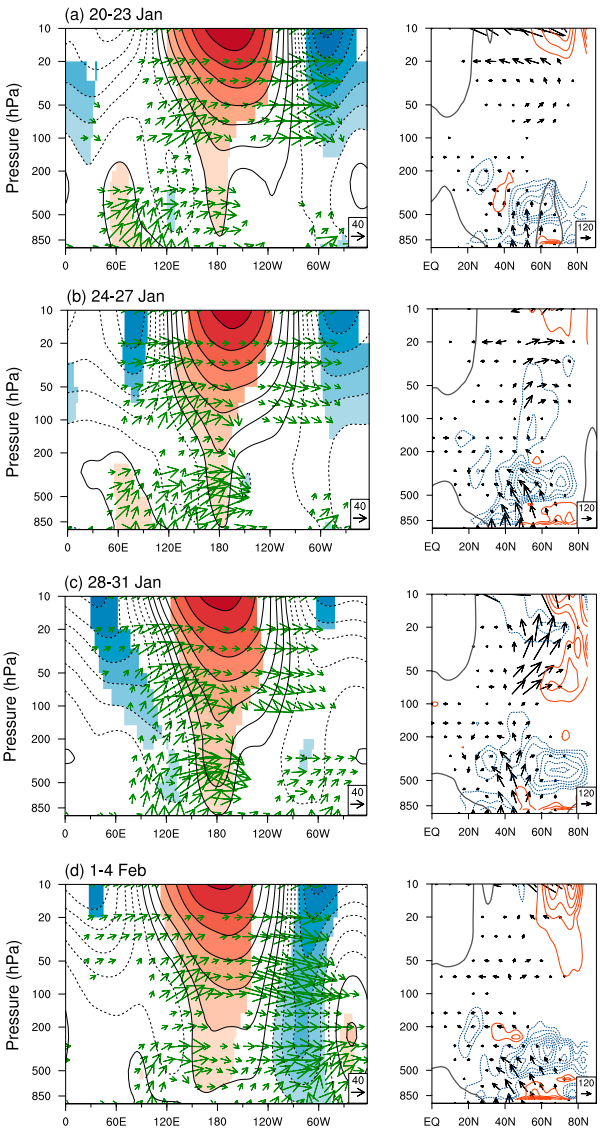

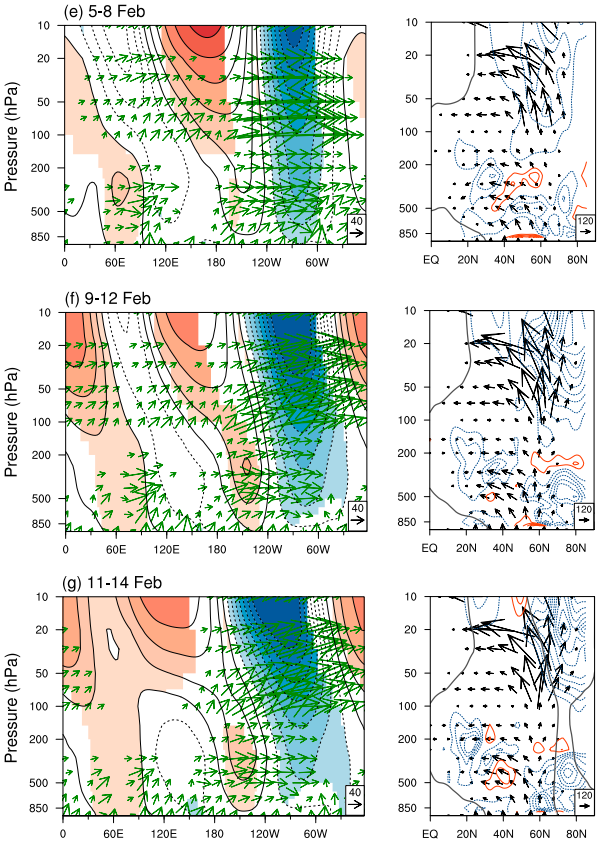

FIG. 7. *(Continued)*

FIG. 7. (left) Successive 4-day means of longitude–pressure cross sections of geopotential height deviations from the zonal mean (contours; 10^2 m) and Plumb wave activity fluxes (vectors; $m^2\,s^{-2}$) averaged over 50°–70°N. The geopotential height deviation contours are shaded only where the statistical significance exceeds the 95% confidence level, based on a Monte Carlo test. (right) Successive 4-day means of latitude–pressure cross sections of zonal-mean zonal wind accelerations (contours; $m\,s^{-2}$) and EP fluxes (vectors; $kg\,s^{-2}$). Vectors are scaled by $\sqrt{1000/p}$ (where p is in hPa). The gray solid lines denote the zero lines of zonal winds. In the left and right panels the contour intervals are 2.0 and 3.0, respectively; the vertical components of the vectors are multiplied by 100 and the vectors above 100 hPa are multiplied by 5; the solid contours denote positive values and the dashed contours denote negative values. The dates are (a) 20–23, (b) 24–27, and (c) 28–31 Jan 2018 and (d) 1–4, (e) 5–8, (f) 9–12, and (g) 11–14 Feb 2018.

dome over Siberia. Based on the potential vorticity conservation (Holton 2004, his section 4.3), anticyclonic (cyclonic) relative vorticity will develop upstream (downstream) of the doming, leading to an upstream high (downstream low) surface pressure response; as the quasi-adiabatic flow follows the raised isentropes, the induced regional form stress provides a local Rossby wave source, allowing the snow-forced cooling to support the increased vertical propagation of PWs from the troposphere into the stratosphere (Cohen et al. 2010; Henderson et al. 2018). Further insight can be gained from the Hovmöller plot of daily temperature anomalies and east–west temperature gradient averaged over 50°–72°N at 850 hPa (Fig. 11d). Similar temperature and gradient distributions are also found at 700 and 500 hPa (not shown). With the presence of positive snow anomalies over Siberia, the land–sea thermal contrast between eastern Eurasia and the Pacific Ocean increases due to anomalous cooling over the land. Therefore, when fluctuating positive snow anomalies occur (Fig. 11d, blue strips on the right), the east–west temperature gradient is strengthened (highlighted by the red frames in Fig. 11d), indicating stronger Rossby wave forcings locally

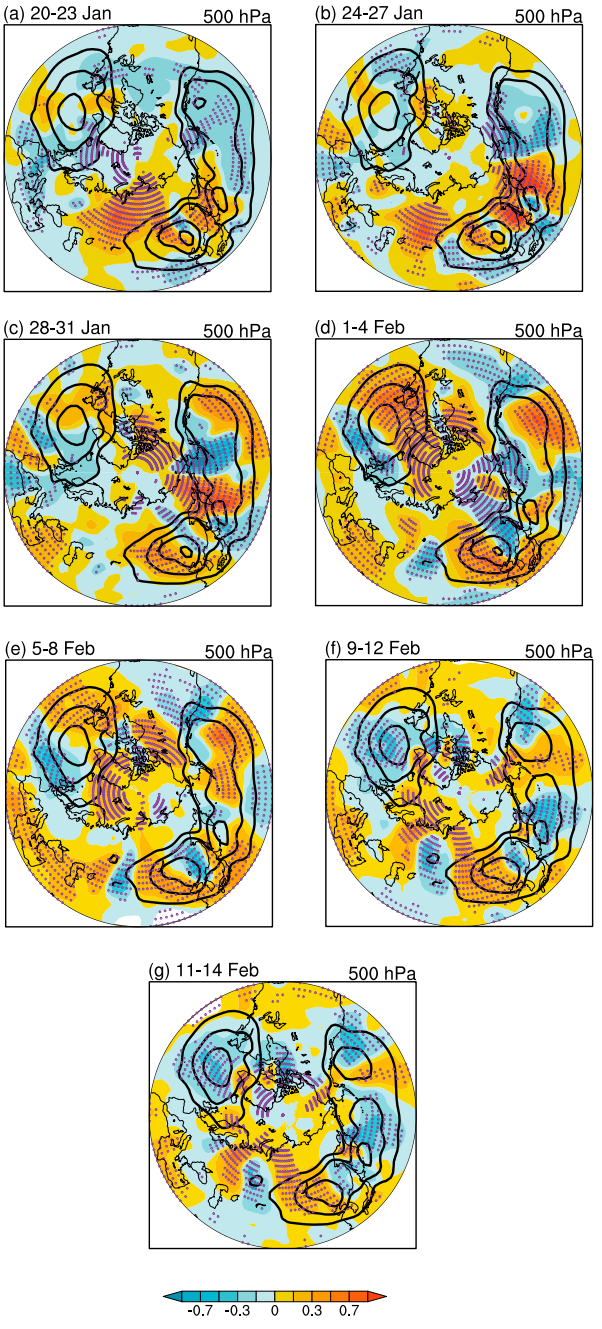

FIG. 8. (a)–(g) The anomalous vertical component of the Plumb wave activity flux (WAFz) at 500 hPa (shading; $m^2 s^{-2}$) during the 7 tetrads from 20 Jan to 14 Feb as in Fig. 7. The dots denote the significant anomalies at the 95% confidence level, based on a Monte Carlo test. The contours indicate the climatology of WAFz ($m^2 s^{-2}$; 0.1–0.4 with interval of 0.1). (h)–(n) Geopotential height anomalies (contours; interval: 10^2 m) and horizontal components of Plumb wave activity fluxes (vectors; $m^2 s^{-2}$) at 250 hPa during the same periods as in (a)–(g). Yellow and blue shadings denote positive and negative anomalies at the 95% significance level, respectively.

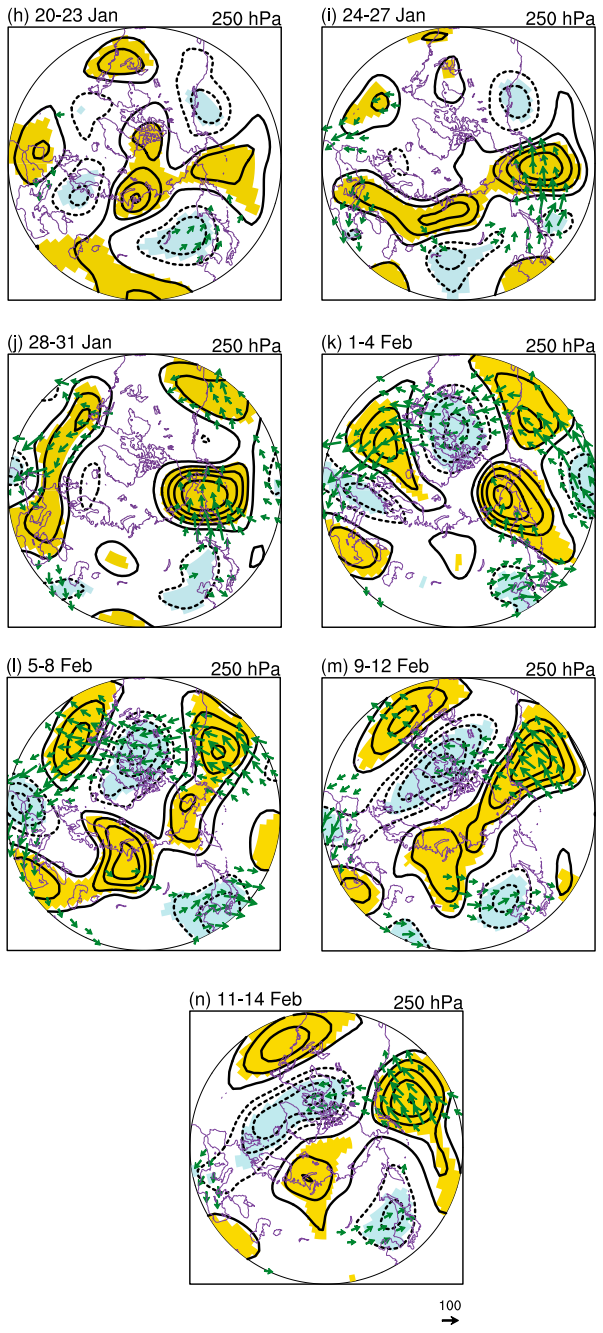

FIG. 8. *(Continued)*

(Hoskins and Karoly 1981). The two pulses of vertical wave-2 heat flux (Fig. 11d, almond strips on the right) occur in the days following the gradient intensification.

4. The snow–SSW linkage over the 2003–19 period

We now examine how the aforementioned connection between Siberian snow depths and the occurrences

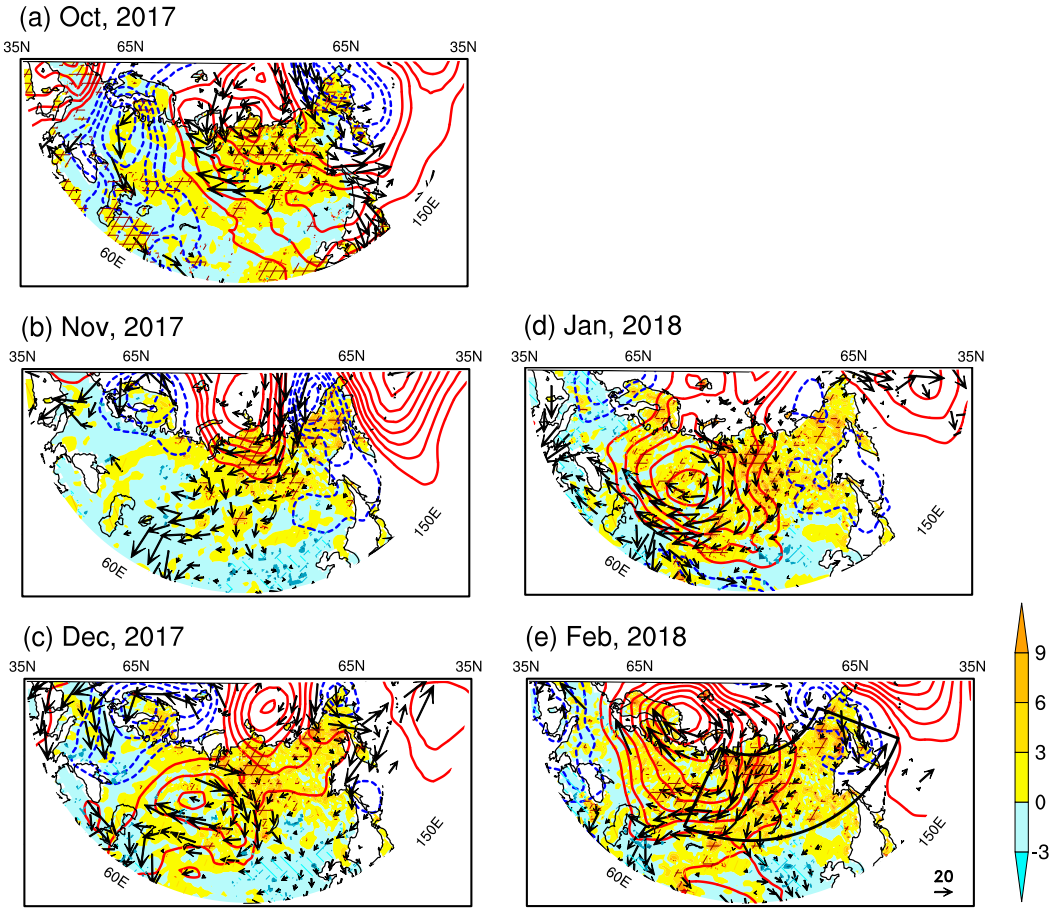

FIG. 9. The monthly anomalies of snow depth (shading; cm), vertically integrated water vapor transport (vectors; kg m^{-1} s^{-1}) from 1000 hPa to 300 hPa, and SLP (contours; hPa) in (a) October, (b) November, and (c) December 2017 and (d) January and (e) February 2018. The snow depth anomalies are cross-hatched only where statistical significance exceeds the 95% confidence level, based on a Monte Carlo test. Solid and dashed contours denote positive and negative values, respectively; the contour intervals are 1.2 for (a) and 2.0 for (b)–(e). The Siberian domain (50°–72°N, 70°–170°E) is indicated by the black frame in (e).

of SSWs holds over a longer period. Given the lack of interannual variability in ERA-Interim snow prior to 2003, our investigation is limited to the last 16 years. While SSWs can happen from November to March with a life cycle on the order of a month, the snow accumulation displays a longer seasonal cycle. Hence, for the intercomparison among the 16 years, a 30-day high-pass filtering was used upon the time series of daily Siberian snow depth anomalies to remove the longer cycle, as shown in Fig. S5 with indications of the maxima. Figure 12 shows the ranked histogram statistics for the maximum daily snow depth anomalies averaged over Siberia during winters from 2003/04 to 2018/19 with indications of winters with or without SSWs (see the explanatory text for details). All eight winters with SSWs had considerable precursory maximum snow mass (above 4.0×10^{12} kg), higher than six out of the eight winters without a SSW although, among years with a SSW, the positive anomaly is above 0.5 standard deviations of the maxima only in the case of three split-type SSWs (indicated by hexagrams). Hence, there is a remarkable finding in Fig. 12, namely that the three split events occurred within the four years when the maximum snow depth was the highest. Although the polar vortex can split in the aftermath of a displacement-type SSW, the three vortex splits correspond to events where the wave 2 dominated prior to the onset, and the split developed nearly simultaneously throughout the stratosphere. This suggests some common traits among the split events, with the aforementioned caveat about causality. It is worth mentioning that in the 2013/14 winter when the third highest snow accumulation occurred, the polar vortex was highly perturbed although no major warming occurred. Kretschmer et al. (2018) argued that this could be due to the more frequent "reflective" rather than "absorbing" polar vortex disruptions.

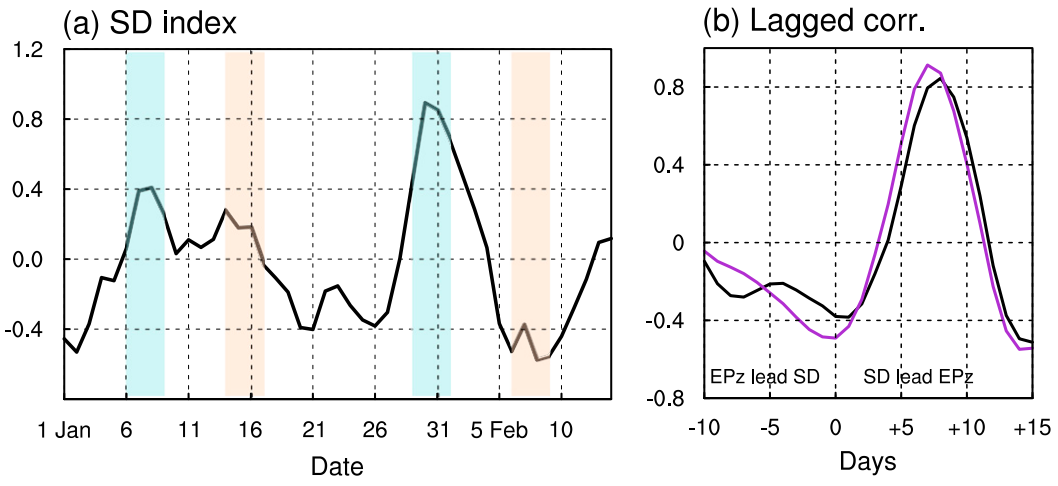

FIG. 10. (a) Time series of normalized Siberian snow depth (SD) index during the period of 1 Jan–10 Feb 2018; the components with periods longer than 30 days are removed after harmonic analysis of Fourier transforms. The blue strips highlight the two major SD pulses while the almond strips highlight the two major $v'T'$_wv2 pulses shown in Fig. 5b. (b) Lead–lag correlations between SD index and normalized magnitude of EPz (black) and EPz_wv2 (purple) at 100 hPa during the same period as in (a).

In the following, the common features of the split events will be examined in more detail. Figure 13a presents the occurrence time and amount of maximum snow depth anomalies and 100-hPa $v'T'$_wv2 anomalies during the three split events in a date–year panel. The daily time series of anomalous snow depth and $v'T'$_wv2 in the three winters are shown together in Fig. S6. As expected during split events, there is unusual development of wave 2 (over +2.0 standard deviations) before the central date. Before the peak wave-2 forcing, however, all the three SSWs are characterized, remarkably, by exceptionally large snow mass with the latter leading the former by approximate one week (Fig. 13a: indicated by the paired dashed lines). After the significantly enhanced snow depth anomalies, wave 2 sharply begins to increase and peak (Fig. S6), indicating lead–lag characteristics similar to those in Fig. 10. Figure 13b shows the composite snow depth and SLP anomalies during 10 to 5 days prior to the occurrence of maximum $v'T'$_wv2. As expected, in this period, anomalous snow accumulation occurs over most of Siberia, with dominant high pressure anomalies across the northern Asian lands. To consider the following troposphere–stratosphere response, we further examine the vertical structure of geopotential height deviation from the zonal mean averaged over 50°–70°N (Fig. 13c). Near the peak of wave-2 heat flux (from −5 to 2 days), a developing ridge is anchored over Siberia, tilting westward with height, consistent with the upward WAF (see also Fig. 7e). Hence, it is the high-latitude positive SLP anomalies, with a high center located in the upstream of significant snow depth anomalies near 90°E (Fig. 13b), that are associated with the enhanced surface-to-stratosphere WAFz. Furthermore, longitude–height cross sections of wave-2 geopotential height anomalies at 60°N also show coherent westward-tilted wave-2 patterns extending from the troposphere to the stratosphere (Fig. S4), consistent with the finding of Coy et al. (2011) about the ridge being anchored to the surface over Siberia before the onset of the 2009 SSW. The in-phase climatological and anomalous wave-2 components indicate constructive interference (as mentioned in section 3b), characteristic of vertical PW propagation into the stratosphere before the central date. Therefore, our analysis documents some common intraseasonal precursors of the three split events, reminiscent of the high SLP-upward WAF linkage by Cohen et al. (2014a) and indicating the importance of surface conditions favored by large snow depth anomalies.

The abovementioned lead–lag relationship is further supported by Fig. 13d, which shows the composite time–height evolution of the anomalous $v'T'$ during the three split-type SSWs. About 2 weeks prior to the central date (from −15 to 0 days), the positive meridional wave-2 heat flux anomalies extend from the surface into the stratosphere (the anomalies are even stronger when waves of all zonal components are included; see Fig. S7). Furthermore, the horizontal distributions of the anomalous 100-hPa WAFz and geopotential height during that period provide a more regional perspective on the tropospheric forcing (Fig. 13e). Over the Siberian sector, where the large snow depth anomalies reside (Fig. 13b), upward-propagating WAFz anomalies are

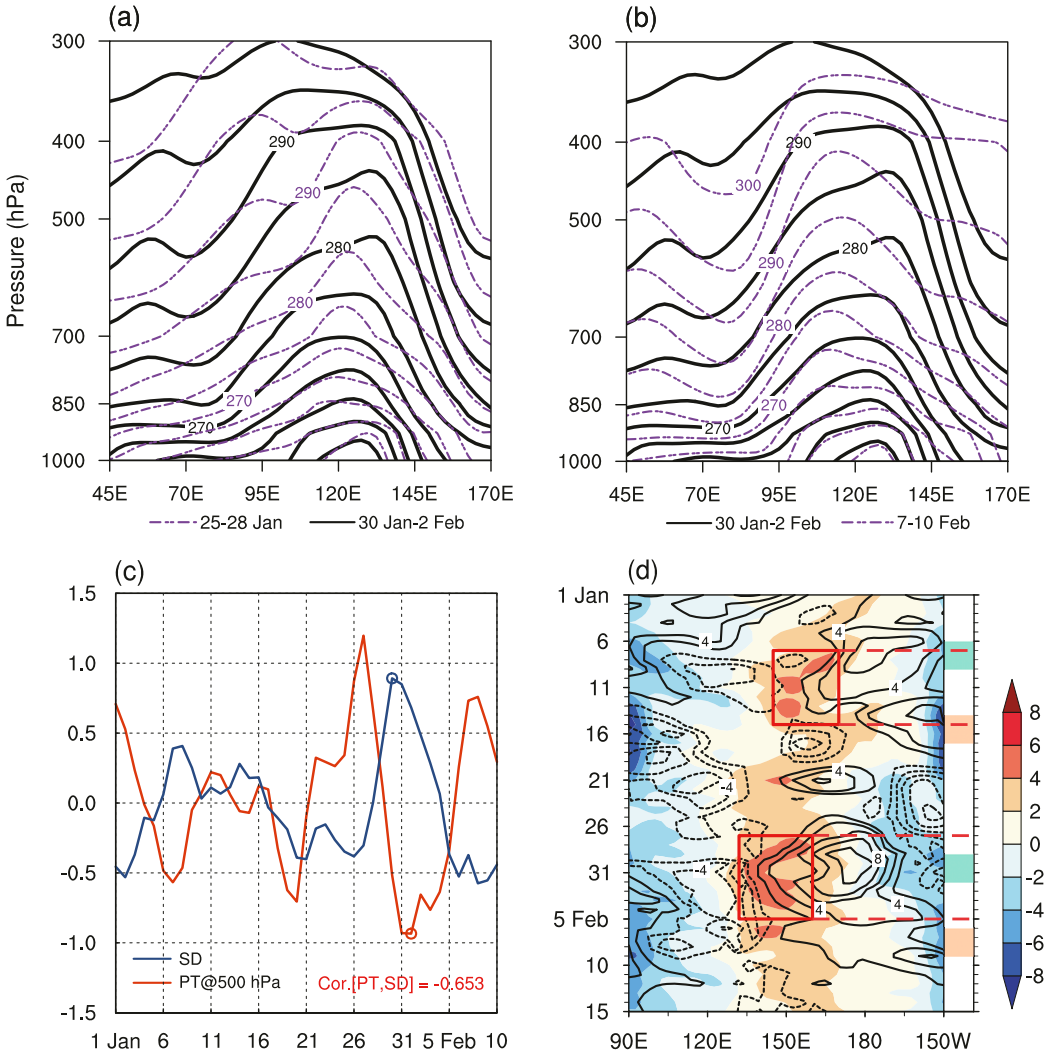

FIG. 11. Longitude–pressure cross sections (meridionally averaged over 50°–72°N) of 4-day means of potential temperature during (a) 25–28 Jan (purple dashed) and 30 Jan–2 Feb (black solid) and (b) 30 Jan–2 Feb (black solid) and 7–10 Feb 2018 (purple dashed). The contour intervals are 5 K. (c) Normalized time series of Siberian SD index and potential temperature (PT) averaged over 50°–72°N, 70°–150°E at 500 hPa during 1 Jan–10 Feb 2018, the components with periods longer than 30 days of both time series are removed. The highest (lowest) value of SD (PT) is marked by a blue (red) circle for reference. (d) Hovmöller plot of daily temperature anomalies (contours; K) and east–west temperature gradient (shading; 10^{-3} K km^{-1}) averaged over the latitude band 50°–72°N at 850 hPa. The red frames highlight the two major gradient intensifications, with the corresponding time indicated by the red dashed lines, while the blue (almond) strips on the right denote the two major SD ($v'T'$_wv2) pulses shown in Fig. 10a.

observed in the upper troposphere. Similar spatial characteristics of the upward WAFz can also be seen at 250 hPa (Fig. S8). In addition, we note that while wave fluxes are also observed over the North American–Atlantic sector sometimes (Fig. 8), their influence is confined to the lower to middle troposphere, and no significant upward anomalies are found there at higher levels (Fig. 13e and Fig. S8).

From the above analyses performed over the past 16 years, the SSWs are linked to preceding Siberian snow anomalies through the setup of amplified vertically propagating PWs from the troposphere into the stratosphere, and this is especially true for the three split-type SSWs. It is possible that when the snow accumulation is large enough (maybe attaining a critical magnitude is necessary), strong upward PW pulses are triggered. This way, the Siberian wave source region, where the climatological wave activity flux maximum is centered, could contribute to the split-type SSW occurrences.

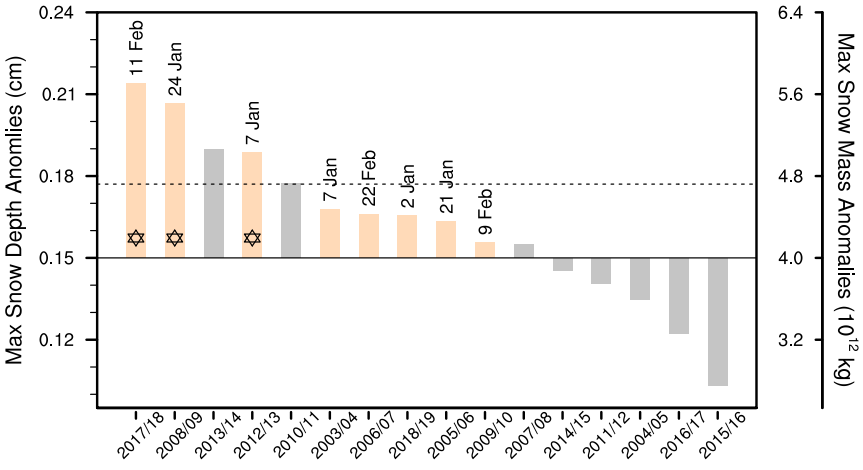

FIG. 12. Distribution of the maximum values of daily snow depth anomalies (cm; 30-day high-passed) averaged over the Siberian region (50°–72°N, 70°–170°E) during the period 2003/04–2018/19, ranking from the highest to the lowest. For the years when a major SSW event occurred (almond bars with central dates above), only snow depth anomalies before the central dates of these SSWs were included; the split-type SSWs are denoted by hexagrams. For the years without an SSW event (gray bars), the maxima were chosen from 1 Dec to 15 Mar to represent the highest snow accumulation extent in winter. The dashed line denotes the level of 0.5 standard deviations above the average. The right *y* axis shows the corresponding snow mass anomalies over Siberia, with a mean snow density of 200 kg m^{-3} assumed.

5. Discussion

A point that should be noted is the attendant role of the tropospheric ridges, including the developed ridge south of Alaska. Here we examine the horizontal propagation of Rossby waves and the evolution of geopotential height anomalies in the mid- to upper troposphere. Emanating from the tropospheric ridge at 50°–120°E (Figs. 7a,b, left; Figs. 8h,i), the eastward-moving wave train transferred their energy from central Asia to the North Pacific, and the ridge over the eastern Pacific began to develop. In early February (Figs. 8l,m), the strengthened ridge migrated farther southeastward to south of Alaska; the ridge characteristic of a Ural blocking developed to the west of the high snow region in the upper troposphere, associated with the westward-tilted wave-2 pattern with height. Therefore, the planetary wave-2 amplification, characterized by the pronounced ridges over the Urals and the eastern Pacific, appears connected to the active wave source over the Siberian region, characterized by thick snowpack and high surface pressure. Specifically, in their Eurasian snow-forced simulation, Orsolini and Kvamsto (2009) found a similar distribution of the Plumb vector vertical component from central Asia to the North Pacific (see their Fig. 8). Based on the above analyses, the snow anomalies over Siberia could stimulate a strong downstream connection in the tropospheric circulation including the strengthened ridge over the eastern Pacific, which was favorable for the maintenance of wave-2 structure. It should be pointed out that the intriguing snow–SSW linkage presented in this study warrants further climate model investigations. While this observational study cannot truly assert causality (it may be that the coincidental development of the two ridges is the cause for both the lagged anomalous snow over Siberia and the SSW), it nevertheless suggests a role for a thick Siberian snowpack, in the key region where the climatological wave activity flux is the strongest, in "anchoring" the wave 2 and favoring its development. Another point worth noting is that while our results provide some necessary information (e.g., the two standard deviations of snow depth anomalies in Fig. 13a), the occurrence of an SSW cannot be absolutely determined by large snow depth, since equally large snow depth amplitudes are observed in a year without an SSW (Fig. S5). It is possible that a static or dynamic threshold of snow fluctuations needs to be reached at a specific time in the seasonal cycle of winter snow accumulation. That characterization remains difficult to quantify based on the short 16-yr datasets, and only three split events. Given the aforementioned caveat about causality, it is possible that there are other confounding factors, like the development of ridges over the Urals, involved in the constructive interference of wave-2 components, and that the snow enhancement of planetary wave activity (e.g., in Fig. 11d) acts as a feedback.

Previous studies indicated that the increased snowfall in the NH continents during winter is often linked to

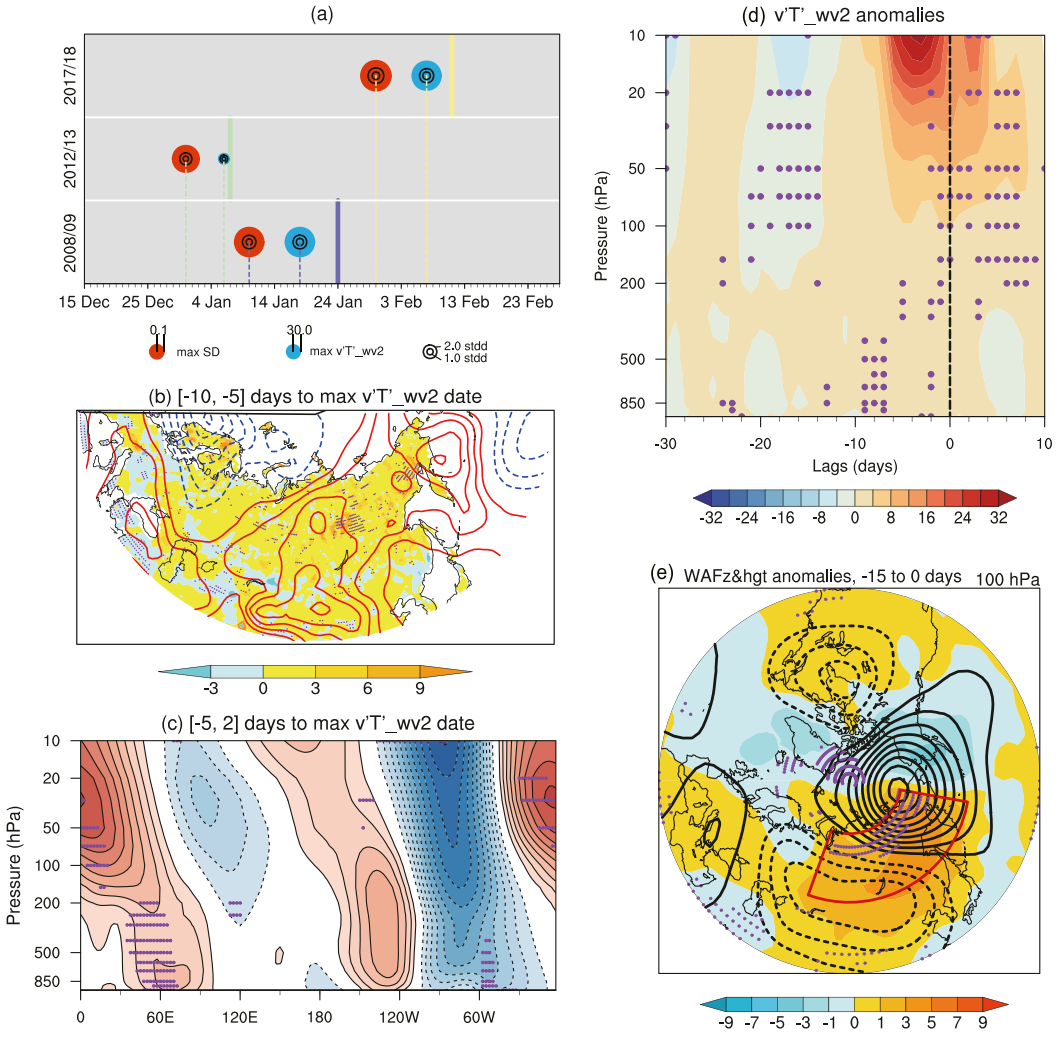

FIG. 13. (a) The occurrence of maximum snow depth (max SD) anomalies and maximum 100-hPa $v'T'$_wv2 anomalies (max $v'T'$_wv2) in the three split SSW events (2017/18, 2012/13, and 2008/09). The radii of the red and blue circles represent the magnitudes of max SD (cm) and max $v'T'$_wv2 (K m s^{-1}), respectively, and the superposed large and small black circles denote spreads of one and two standard deviations, respectively. The thick vertical colored line displays the central date and the dashed vertical lines indicate the occurrence time of max SD and max $v'T'$_wv2. (b) Composite snow depth (shading; cm) and SLP (contours; interval: 2.0 hPa) anomalies from 10 to 5 days before the occurrence date of max $v'T'$_wv2 for the three split events. (c) Composite daily normalized anomalies of geopotential height deviation from the zonal mean averaged over 50°–70°N (interval: 0.2) from −5 to 2 days around the occurrence date of max $v'T'$_wv2. (d) Time–pressure cross section of composite zonal-mean $v'T'$ anomalies (10 K m s^{-1}) of wave 2 averaged over 30°–90°N from −30 to 10 days around the central date of the three SSWs. (e) Composite WAFz anomalies (shading; 10^{-2} m^2 s^{-2}) and geopotential height anomalies (contours; interval: 30 m) at 100 hPa from 15 to 0 days before the central date. The purple dots in (b)–(e) denote the significant anomalies at the 90% confidence level, based on the Student's t test. The red frame in (e) denotes the Siberian region.

diminishing autumn Arctic sea ice through changing atmospheric water vapor content and circulation transport (Liu et al. 2012; Gao et al. 2015; Wegmann et al. 2015). Here, the monthly spatial distributions of the Arctic sea ice concentration (SIC) anomalies (Figs. S9a–e) show that in late autumn and winter of 2017/18, anomalous low SIC existed over most of the Arctic seas, especially the Atlantic sectors of the Arctic seas and the Chukchi–Bering Seas. Low Arctic sea ice extent is favorable for large specific humidity increases through enhanced turbulent heat flux (Screen and Simmonds 2010), which can induce additional moisture transport to adjacent continents and snow accumulation over Siberia (Wegmann et al. 2015). The scatterplot (Fig. S9f) indicates significant decreasing trend of SIC in the Barents–Kara–Laptev Seas. Oppositely, the southward

WVT anomalies across the Siberian coast display a quantitative increase in the past four decades. The southward WVT of January 2018 was at a relatively high level (the third highest during 1979–2018), indicating a possible linkage between the low SIC and large snow accumulation in midwinter of 2018. Therefore, the low Arctic sea ice conditions could provide further support for the connection between enhanced snow depths and more frequent polar vortex split events in recent years, although a detailed analysis remains to be done.

6. Summary

The weather in late February 2018 was particularly severe for many of the populous centers of Europe. The severe winter weather was associated with the major SSW event occurring on 11 February 2018, accompanied by an anomalous NAO− pattern. This study extends the previous work (e.g., Cohen et al. 2007; Harada et al. 2010), linking anomalous Siberian snow depth to the European cold extremes via this SSW event on subseasonal time scales.

In particular, we have focused on the linkage between time-evolving Siberian snow depth anomaly and the troposphere–stratosphere coupling, which is further identified on daily time scales. Based on our results, we argue that the snow-driven atmospheric changes and the induced upward-propagating PWs mainly occur after large snow depth anomalies. During the winter of 2017/18, a heavy snow accumulation occurred over the northern Eurasia, especially over Siberia. Two large Siberian snow depth anomalies occurring in early and late January corresponded to two positive pulses of upward PWs (mainly wave-2 PWs) into the stratosphere, on a time scale of approximate one week (i.e., 7–8 days). The persistent wave activity triggered the onset of SSW18 and an ensuing vortex splitting via wave–mean flow interaction. We also find that the snow–split event linkages in 2013 and 2009 bear similarities to that in SSW18. Large snow depth anomaly maxima precede the wave-2 anomaly maxima by about a week, occurring prior to the central date of SSW.

Early predictions of the stratospheric polar state are important to improve forecasts of mid- to high-latitude extreme weather including cold spells. The precursory snow increases described here could potentially improve forecast at the subseasonal time scale, irrespective of whether there is causality or not between snow anomalies and occurrence of the SSW. Siberian snow anomalies have in fact been included as a potential predictor of the NAO and stratospheric variability [see Cohen et al. (2014b) or Henderson et al. (2018) for reviews]. However, the failure of climate models to represent the magnitude of the observed snow interannual variability over Eurasia, and to simulate a realistic response to snow cover variations and snow–stratosphere linkages (Hardimann et al. 2008; Peings et al. 2012; Henderson et al. 2018), would imply that such extreme occurrences might be missed in climate scenario simulations. In a case study of the 2009/10 winter using a high-resolution operational seasonal forecast model, Orsolini et al. (2016) did show that both the PW flux and the stratospheric polar vortex strength were rapidly modulated by the snow cover. The current study is also indicative of a PW flux and vortex response to the eastern Eurasia mean snow depth variations (e.g., Fig. 10, with a lag near a week). A remarkable association between occurrences of vortex split events and high Siberian snow depths is found over the last 16 years (Fig. 12). Nevertheless, the precise causal attribution of the planetary wave response to the snow variations is still a challenge, which needs to be addressed with dedicated climate or forecast model simulations. The robustness of these results over the longer term needs to be further assessed in the future, using high-quality snow analysis products and controlled, improved model simulations.

Acknowledgments. This research was supported by National Natural Science Foundation of China (Grants 41421004, 41605059 and 41505073) and the National Key Research and Development Program of China (Grant 2016YFA0600703). YOR was supported by the Research Council of Norway (Grant SNOWGLACE 244166). Y. Q. Gao was funded by the EU H2020 Blue-Action project (grant 727852). Z Z. Lü also benefited from the Research Council of Norway (Grant INTPART-ARCONOR 261743).

REFERENCES

Anadolu Agency, 2018: Record-setting cold weather continues to grip Europe. Accessed 5 November 2018, https://www.aa.com.tr/en/europe/record-setting-cold-weather-continues-to-grip-europe/1077623.

Andrews, D. G., J. R. Holton, and C. B. Leovy, 1987: *Middle Atmosphere Dynamics*. Academic Press, 489 pp.

Ano plc, 2018: Global Catastrophe Recap. Accessed 5 November 2018, 16 pp., http://thoughtleadership.aonbenfield.com//Documents/20190118-ab-if-december- global-recap.pdf.

Ayarzagüena, B., D. Barriopedro, J. M. Garrido-Perez, M. Abalos, A. de la Cámara, R. García-Herrera, N. Calvo, and C. Ordóñez, 2018: Stratospheric connection to the abrupt end of the 2016/2017 Iberian drought. *Geophys. Res. Lett.*, **45**, 12 639–12 646, https://doi.org/10.1029/2018GL079802.

Betts, A. K., R. Desjardins, D. Worth, S. S. Wang, and J. H. Li, 2014: Coupling of winter climate transitions to snow and clouds over the Prairies. *J. Geophys. Res.*, **119**, 1118–1139, https://doi.org/10.1002/2013JD021168.

Buehler, T., C. C. Raible, and T. F. Stocker, 2011: The relationship of winter season North Atlantic blocking frequencies to extreme cold or dry spells in the ERA-40. *Tellus*, **63A**, 174–187, https://doi.org/10.1111/j.1600-0870.2010.00492.x.

Butler, A. H., D. J. Seidel, S. C. Hardiman, N. Butchart, T. Birner, and A. Match, 2015: Defining sudden stratospheric warmings. *Bull. Amer. Meteor. Soc.*, **96**, 1913–1928, https://doi.org/10.1175/BAMS-D-13-00173.1.

——, J. P. Sjoberg, D. J. Seidel, and K. H. Rosenlof, 2017: A sudden stratospheric warming compendium. *Earth Syst. Sci. Data*, **9**, 63–76, https://doi.org/10.5194/essd-9-63-2017.

Cattiaux, J., R. Vautard, C. Cassou, P. Yiou, V. Masson-Delmotte, and F. Codron, 2010: Winter 2010 in Europe: A cold extreme in a warming climate. *Geophys. Res. Lett.*, **37**, L20704, https://doi.org/10.1029/2010GL044613.

Charlton, A. J., and L. M. Polvani, 2007: A new look at stratospheric sudden warmings. Part I: Climatology and modeling benchmarks. *J. Climate*, **20**, 449–469, https://doi.org/10.1175/JCLI3996.1.

Charney, J. G., and P. G. Drazin, 1961: Propagation of planetary-scale disturbances from the lower into the upper atmosphere. *J. Geophys. Res.*, **66**, 83–109, https://doi.org/10.1029/JZ066i001p00083.

Chen, W., M. Takahashi, and H. F. Graf, 2003: Interannual variations of stationary planetary wave activity in the northern winter troposphere and stratosphere and their relations to NAM and SST. *J. Geophys. Res.*, **108**, 4797, https://doi.org/10.1029/2003JD003834.

Cheung, H. H. N., W. Zhou, M. Y. T. Leung, C. M. Shun, S. M. Lee, and H. W. Tong, 2016: A strong phase reversal of the Arctic Oscillation in midwinter 2015/2016: Role of the stratospheric polar vortex and tropospheric blocking. *J. Geophys. Res.*, **121**, 13 443–13 457, https://doi.org/10.1002/2016JD025288.

Cohen, J., and D. Entekhabi, 1999: Eurasian snow cover variability and Northern Hemisphere climate predictability. *Geophys. Res. Lett.*, **26**, 345–348, https://doi.org/10.1029/1998GL900321.

——, ——, K. Saito, G. Gong, and D. Salstein, 2005: Comments on "The life cycle of the Northern Hemisphere sudden stratospheric warmings." *J. Climate*, **18**, 2775–2777, https://doi.org/10.1175/JCLI3443.1.

——, M. Barlow, P. J. Kushner, and K. Saito, 2007: Stratosphere–troposphere coupling and links with Eurasian land surface variability. *J. Climate*, **20**, 5335–5343, https://doi.org/10.1175/2007JCLI1725.1.

——, J. Foster, M. Barlow, K. Saito, and J. Jones, 2010: Winter 2009–2010: A case study of an extreme Arctic Oscillation event. *Geophys. Res. Lett.*, **37**, L17707, https://doi.org/10.1029/2010GL044256.

——, J. C. Furtado, J. Jones, M. Barlow, D. Whittleston, and D. Entekhabi, 2014a: Linking Siberian snow cover to precursors of stratospheric variability. *J. Climate*, **27**, 5422–5432, https://doi.org/10.1175/JCLI-D-13-00779.1.

——, and Coauthors, 2014b: Recent Arctic amplification and extreme mid-latitude weather. *Nat. Geosci.*, **7**, 627–637, https://doi.org/10.1038/ngeo2234.

Coy, L., S. D. Eckermann, K. W. Hoppel, and F. Sassi, 2011: Mesospheric precursors to the major stratospheric sudden warming of 2009: Validation and dynamical attribution using a ground-to-edge-of-space data assimilation system. *J. Adv. Model. Earth Syst.*, **3**, M10002, https://doi.org/10.1029/2011MS000067.

Dee, D. P., and Coauthors, 2011: The ERA-Interim reanalysis: Configuration and performance of the data assimilation system. *Quart. J. Roy. Meteor. Soc.*, **137**, 553–597, https://doi.org/10.1002/qj.828.

Douville, H., Y. Peings, and D. Saint-Martin, 2017: Snow–(N)AO relationship revisited over the whole twentieth century. *Geophys. Res. Lett.*, **44**, 569–577, https://doi.org/10.1002/2016GL071584.

Fletcher, C. G., S. C. Hardiman, P. J. Kushner, and J. Cohen, 2009: The dynamical response to snow cover perturbations in a large ensemble of atmospheric GCM integrations. *J. Climate*, **22**, 1208–1222, https://doi.org/10.1175/2008JCLI2505.1.

Furtado, J. C., J. L. Cohen, and E. Tziperman, 2016: The combined influences of autumnal snow and sea ice on Northern Hemisphere winters. *Geophys. Res. Lett.*, **43**, 3478–3485, https://doi.org/10.1002/2016GL068108.

Gao, Y., and Coauthors, 2015: Arctic sea ice and Eurasian climate: A review. *Adv. Atmos. Sci.*, **32**, 92–114, https://doi.org/10.1007/s00376-014-0009-6.

Gong, G., D. Entekhabi, and J. Cohen, 2003: Modeled Northern Hemisphere winter climate response to realistic Siberian snow anomalies. *J. Climate*, **16**, 3917–3931, https://doi.org/10.1175/1520-0442(2003)016<3917:MNHWCR>2.0.CO;2.

——, ——, ——, and D. Robinson, 2004: Sensitivity of atmospheric response to modeled snow anomaly characteristics. *J. Geophys. Res.*, **109**, D06107, https://doi.org/10.1029/2003JD004160.

Harada, Y., A. Goto, H. Hasegawa, N. Fujikawa, H. Naoe, and T. Hirooka, 2010: A major stratospheric sudden warming event in January 2009. *J. Atmos. Sci.*, **67**, 2052–2069, https://doi.org/10.1175/2009JAS3320.1.

Hardiman, S. C., P. J. Kushner, and J. Cohen, 2008: Investigating the ability of general circulation models to capture the effects of Eurasian snow cover on winter climate. *J. Geophys. Res.*, **113**, D21123, https://doi.org/10.1029/2008JD010623.

Henderson, G. R., Y. Peings, J. C. Furtado, and P. J. Kushner, 2018: Snow–atmosphere coupling in the Northern Hemisphere. *Nat. Climate Change*, **8**, 954–963, https://doi.org/10.1038/s41558-018-0295-6.

Holton, J. R., 2004: *An Introduction to Dynamic Meteorology*. Academic Press, 535 pp.

Hoskins, B. J., and D. J. Karoly, 1981: The steady linear response of a spherical atmosphere to thermal and orographic forcing. *J. Atmos. Sci.*, **38**, 1179–1196, https://doi.org/10.1175/1520-0469(1981)038<1179:TSLROA>2.0.CO;2.

Hurrell, J. W., 1995: Decadal trends in the North Atlantic Oscillation: Regional temperatures and precipitation. *Science*, **269**, 676–679, https://doi.org/10.1126/science.269.5224.676.

Kanamitsu, M., W. Ebisuzaki, J. Woollen, S. K. Yang, J. J. Hnilo, M. Fiorino, and G. L. Potter, 2002: NCEP–DOE AMIP-II reanalysis (R-2). *Bull. Amer. Meteor. Soc.*, **83**, 1631–1643, https://doi.org/10.1175/BAMS-83-11-1631.

Kidston, J., A. A. Scaife, S. C. Hardiman, D. M. Mitchell, N. Butchart, M. P. Baldwin, and L. J. Gray, 2015: Stratospheric influence on tropospheric jet streams, storm tracks and surface weather. *Nat. Geosci.*, **8**, 433–440, https://doi.org/10.1038/ngeo2424.

Kretschmer, M., J. Cohen, V. Matthias, J. Runge, and D. Coumou, 2018: The different stratospheric influence on cold-extremes in Eurasia and North America. *npj Climate Atmos. Sci.*, **1**, 44, https://doi.org/10.1038/s41612-018-0054-4.

Lamb, P. J., and R. A. Peppler, 1987: North Atlantic Oscillation: Concept and an application. *Bull. Amer. Meteor. Soc.*, **68**, 1218–1225, https://doi.org/10.1175/1520-0477(1987)068<1218:NAOCAA>2.0.CO;2.

Lapin, T., 2018: Deadly storm dubbed "Beast from the East" pounds Europe. *New York Post*, 27 February 2018, https://nypost.com/2018/02/27/deadly-storm-dubbed-beast-from-the-east-pounds-europe/amp/.

Li, F., H. Wang, and Y. Gao, 2015: Extratropical ocean warming and winter Arctic sea ice cover since the 1990s. *J. Climate*, **28**, 5510–5522, https://doi.org/10.1175/JCLI-D-14-00629.1.

——, Y. J. Orsolini, H. Wang, Y. Gao, and S. He, 2018: Atlantic multidecadal oscillation modulates the impacts of Arctic sea ice decline. *Geophys. Res. Lett.*, **45**, 2497–2506, https://doi.org/10.1002/2017GL076210.

——, ——, N. Keenlyside, M. L. Shen, F. Counillon, and Y. G. Wang, 2019: Impact of snow initialization in subseasonal-to-seasonal winter forecasts with the Norwegian Climate Prediction Model. *J. Geophys. Res. Atmos.*, **124**, 10 033–10 048, https://doi.org/10.1029/2019JD030903.

Limpasuvan, V., D. W. J. Thompson, and D. L. Hartmann, 2004: The life cycle of the Northern Hemisphere sudden stratospheric warmings. *J. Climate*, **17**, 2584–2596, https://doi.org/10.1175/1520-0442(2004)017<2584:TLCOTN>2.0.CO;2.

——, ——, and ——, 2005: Reply. *J. Climate*, **18**, 2778–2780, https://doi.org/10.1175/JCLI3444.1.

Liu, J., J. A. Curry, H. Wang, M. Song, and R. M. Horton, 2012: Impact of declining Arctic sea ice on winter snowfall. *Proc. Natl. Acad. Sci. USA*, **109**, 4074–4079, https://doi.org/10.1073/pnas.1114910109.

Manzini, E., M. A. Giorgetta, M. Esch, L. Kornblueh, and E. Roeckner, 2006: The influence of sea surface temperatures on the northern winter stratosphere: Ensemble simulations with the MAECHAM5 model. *J. Climate*, **19**, 3863–3881, https://doi.org/10.1175/JCLI3826.1.

Matsuno, T., 1971: A dynamical model of the stratospheric sudden warming. *J. Atmos. Sci.*, **28**, 1479–1494, https://doi.org/10.1175/1520-0469(1971)028<1479:ADMOTS>2.0.CO;2.

McInturff, R. M., 1978: Stratospheric warmings: Synoptic, dynamic and general-circulation aspects. NASA Tech. Rep. NASA-RP-1017, 173 pp.

Mitchell, D. M., L. J. Gray, J. Anstey, M. P. Baldwin, and A. J. Charlton-Perez, 2013: The influence of stratospheric vortex displacements and splits on surface climate. *J. Climate*, **26**, 2668–2682, https://doi.org/10.1175/JCLI-D-12-00030.1.

Moses, T., G. N. Kiladis, H. F. Diaz, and R. G. Barry, 1987: Characteristics and frequency of reversals in mean sea level pressure in the North Atlantic sector and their relationship to long-term temperature trends. *J. Climatol.*, **7**, 13–30, https://doi.org/10.1002/joc.3370070104.

Nath, D., W. Chen, C. Zelin, A. I. Pogoreltsev, and K. Wei, 2016: Dynamics of 2013 sudden stratospheric warming event and its impact on cold weather over Eurasia: Role of planetary wave reflection. *Sci. Rep.*, **6**, 24174, https://doi.org/10.1038/srep24174.

Nishii, K., H. Nakamura, and Y. J. Orsolini, 2011: Geographical dependence observed in blocking high influence on the stratospheric variability through enhancement and suppression of upward planetary-wave propagation. *J. Climate*, **24**, 6408–6423, https://doi.org/10.1175/JCLI-D-10-05021.1.

Orsolini, Y. J., and N. G. Kvamsto, 2009: Role of Eurasian snow cover in wintertime circulation: Decadal simulations forced with satellite observations. *J. Geophys. Res.*, **114**, D19108, https://doi.org/10.1029/2009JD012253.

——, R. Senan, G. Balsamo, F. J. Doblas-Reyes, F. Vitart, A. Weisheimer, A. Carrasco, and R. E. Benestad, 2013: Impact of snow initialization on sub-seasonal forecasts. *Climate Dyn.*, **41**, 1969–1982, https://doi.org/10.1007/s00382-013-1782-0.

——, ——, F. Vitart, G. Balsamo, A. Weisheimer, and F. J. Doblas-Reyes, 2016: Influence of the Eurasian snow on the negative North Atlantic Oscillation in subseasonal forecasts of the cold winter 2009/2010. *Climate Dyn.*, **47**, 1325–1334, https://doi.org/10.1007/s00382-015-2903-8.

——, K. Nishii, and H. Nakamura, 2018: Duration and decay of Arctic stratospheric vortex events in the ECMWF seasonal forecast model. *Quart. J. Roy. Meteor. Soc.*, **144**, 2876–2888, https://doi.org/10.1002/qj.3417.

Peings, Y., D. Saint-Martin, and H. Douville, 2012: A numerical sensitivity study of the influence of Siberian snow on the northern annular mode. *J. Climate*, **25**, 592–607, https://doi.org/10.1175/JCLI-D-11-00038.1.

Pfahl, S., 2014: Characterising the relationship between weather extremes in Europe and synoptic circulation features. *Nat. Hazards Earth Syst. Sci.*, **14**, 1461–1475, https://doi.org/10.5194/nhess-14-1461-2014.

Plumb, R. A., 1985: On the three-dimensional propagation of stationary waves. *J. Atmos. Sci.*, **42**, 217–229, https://doi.org/10.1175/1520-0469(1985)042<0217:OTTDPO>2.0.CO;2.

Polvani, L. M., and D. W. Waugh, 2004: Upward wave activity flux as a precursor to extreme stratospheric events and subsequent anomalous surface weather regimes. *J. Climate*, **17**, 3548–3554, https://doi.org/10.1175/1520-0442(2004)017<3548:UWAFAA>2.0.CO;2.

Saito, K., and J. Cohen, 2003: The potential role of snow cover in forcing interannual variability of the major Northern Hemisphere mode. *Geophys. Res. Lett.*, **30**, 1302, https://doi.org/10.1029/2002GL016341.

——, ——, and D. Entekhabi, 2001: Evolution of atmospheric response to early-season Eurasian snow cover anomalies. *Mon. Wea. Rev.*, **129**, 2746–2760, https://doi.org/10.1175/1520-0493(2001)129<2746:EOARTE>2.0.CO;2.

Screen, J. A., and I. Simmonds, 2010: The central role of diminishing sea ice in recent Arctic temperature amplification. *Nature*, **464**, 1334–1337, https://doi.org/10.1038/nature09051.

Seviour, W. J. M., D. M. Mitchell, and L. J. Gray, 2013: A practical method to identify displaced and split stratospheric polar vortex events. *Geophys. Res. Lett.*, **40**, 5268–5273, https://doi.org/10.1002/grl.50927.

Sillmann, J., M. Croci-Maspoli, M. Kallache, and R. W. Katz, 2011: Extreme cold winter temperatures in Europe under the influence of North Atlantic atmospheric blocking. *J. Climate*, **24**, 5899–5913, https://doi.org/10.1175/2011JCLI4075.1.

Smith, K. L., P. J. Kushner, and J. Cohen, 2011: The role of linear interference in northern annular mode variability associated with Eurasian snow cover extent. *J. Climate*, **24**, 6185–6202, https://doi.org/10.1175/JCLI-D-11-00055.1.

Taguchi, M., 2014: Predictability of major stratospheric sudden warmings of the vortex split type: Case study of the 2002 southern event and the 2009 and 1989 northern events. *J. Atmos. Sci.*, **71**, 2886–2904, https://doi.org/10.1175/JAS-D-13-078.1.

Takaya, K., and H. Nakamura, 2005: Mechanisms of intraseasonal amplification of the cold Siberian high. *J. Atmos. Sci.*, **62**, 4423–4440, https://doi.org/10.1175/JAS3629.1.

Thompson, D. W. J., and J. M. Wallace, 1998: The Arctic Oscillation signature in the wintertime geopotential height and temperature fields. *Geophys. Res. Lett.*, **25**, 1297–1300, https://doi.org/10.1029/98GL00950.

Wegmann, M., and Coauthors, 2015: Arctic moisture source for Eurasian snow cover variations in autumn. *Environ. Res. Lett.*, **10**, 054015, https://doi.org/10.1088/1748-9326/10/5/054015.

Wilks, D. S., 2006: *Statistical Methods in the Atmospheric Sciences*. 2nd ed. Academic Press, 627 pp.

Zhang, J., W. Tian, M. P. Chipperfield, F. Xie, and J. Huang, 2016: Persistent shift of the Arctic polar vortex towards the Eurasian continent in recent decades. *Nat. Climate Change*, **6**, 1094–1099, https://doi.org/10.1038/nclimate3136.

Zhang, X. B., G. Hegerl, F. W. Zwiers, and J. Kenyon, 2005: Avoiding inhomogeneity in percentile-based indices of temperature extremes. *J. Climate*, **18**, 1641–1651, https://doi.org/10.1175/JCLI3366.1.